Structural Effects on the Biodistribution and Positron Emission Tomography (PET) Imaging of Well-Defined ^{64}Cu-Labeled Nanoparticles Comprised of Amphiphilic Block Graft Copolymers

Eric D. Pressly,[†,⊥] Raffaella Rossin,[‡,⊥] Aviv Hagooly,[‡] Ken-ichi Fukukawa,[†] Benjamin W. Messmore,[†] Michael J. Welch,[*,‡,§] Karen L. Wooley,[*,‡,§] Matthew S. Lamm,[||] Rohan A. Hule,[||] Darrin J. Pochan,[||] and Craig J. Hawker[*,†]

Materials Research Laboratory, Departments of Chemistry, Biochemistry and Materials, University of California, Santa Barbara, California 93106, Divisions of Chemistry and Radiological Sciences, Washington University, St. Louis, Missouri 63110, and Materials Science and Engineering, University of Delaware, Newark, Delaware 19716

Received May 16, 2007; Revised Manuscript Received July 30, 2007

The synthesis of poly(methyl methacrylate-*co*-methacryloxysuccinimide-*graft*-poly(ethylene glycol)) (PMMA-*co*-PMASI-*g*-PEG) via living free radical polymerization provides a convenient route to well-defined amphiphilic graft copolymers having a controllable number of reactive functional groups, variable length PEG grafts, and low polydispersity. These copolymers were shown to form PMMA-core/PEG-shell nanoparticles upon hydrophobic collapse in water, with the hydrodynamic size being defined by the molecular weight of the backbone and the PEG grafts. Functionalization of these polymeric nanoparticles with a 1,4,7,10-tetraazacyclododecanetetraacetic acid (DOTA) ligand capable of chelating radioactive ^{64}Cu nuclei enabled the biodistribution and *in vivo* positron emission tomography of these materials to be studied and directly correlated to the initial structure. Results indicate that nanoparticles with increasing PEG chain lengths show increased blood circulation and low accumulation in excretory organs, suggesting the possible use of these materials as stealth carriers for medical imaging and systemic administration.

Introduction

Over the past decade, the ability to prepare well-defined nanostructures has allowed the field of nanomedicine to emerge as an exciting area of interest for researchers in areas ranging from chemical synthesis to diagnostics and related clinical studies. With an expected market for nanomedical products of approximately $12 billion in 2012,[1] there is a growing need for fundamental structure/property relationships to be developed for the biological function of these nanomaterials which underscores the necessity for well-defined chemical approaches to these systems.[2] In terms of synthetic ease and accessibility, the design and preparation of well-defined polymeric nanostructures offer several advantages over small-molecule counterparts, including multivalent display of chemical signals, size on the scale of proteins and cellular structures, and the capability to carry and release a therapeutic payload in a controlled fashion. Traditionally, a major limitation in the use of polymeric nanoparticles *in vivo* is their premature elimination from the circulatory system by the mononuclear phagocyte system (MPS), which can rapidly remove them from the bloodstream and prevent the nanoparticles from reaching their target.[3] The disposal of particles through the MPS follows a complex pathway beginning with the adsorption of serum proteins (opsonins) onto the surface of the nanoparticle, followed by macrophage recognition, phagocytosis, and subsequent sequestration in the liver, spleen, and bone marrow.[4] The elucidation of design parameters, for example, molecular weight, core shell architecture, and so forth, of functionalized nanoparticles that can avoid opsonin adsorption and thereby slow down their elimination by the MPS is a critical first step in the development of targeted nanoparticle imaging agents for a variety of heart, lung, and blood injuries. In all of these diagnostic applications, long blood circulation is needed to achieve ligand−receptor equilibrium.

Among the various strategies to increase blood circulation lifetimes of biomaterials, poly(ethylene glycol) (PEG) has emerged as a leading candidate to minimize the MPS response.[2−8] PEG is an uncharged, hydrophilic, nonimmunogenic polymer approved for human use,[9] and it can be physically adsorbed or covalently grafted onto the surface of nanoparticles.[5,8] Though the mechanism responsible for the stealth properties of PEG-coated particles is still controversial,[10] the influence of surface density and PEG chain length on the interaction of nanoparticles with plasma proteins and macrophages is confirmed *in vitro*[5−8,11] and prolonged blood circulation of PEGylated nanosystems is observed *in vivo*.[2,3,5,8,10,12,13]

A number of strategies have been recently developed to prepare polymeric nanostructures with a surface coverage of PEG.[14−16] For example, micelles formed by amphiphilic diblock copolymers with PEG as the hydrophilic block have been reported to hold hydrophobic payloads and contrast agents.[17−21] Herein, we report the synthesis via reversible addition fragmentation transfer (RAFT) polymerization of high molecular

* To whom correspondence should be addressed. Telephone: (805) 893-7161. Fax: (805) 893-8797. E-mail: hawker@mrl.ucsb.edu.
† University of California, Santa Barbara.
‡ Division of Radiological Sciences, Washington University School of Medicine.
§ Division of Chemistry, Washington University.
|| University of Delaware.
⊥ These authors contributed equally to this work.

10.1021/bm700541e CCC: $37.00
Published on Web 09/20/2007

weight PEG graft copolymers containing a hydrophobic methyl methacrylate backbone with reactive functional groups for the attachment of diagnostic positron emitting moieties. By controlling the molecular structure of these comb copolymers, a controlled collapse of the hydrophobic backbone to form well-defined nanoparticles in aqueous solution is observed and variation of the length of the PEG grafts allows a structure/property profile for the pharmacokinetics and enhanced blood lifetime to be developed.

Experimental Procedures

Materials. Chemicals were purchased from Sigma-Aldrich (St. Louis, MO) and used without further purification unless otherwise stated, and functionalized poly(ethylene glycol) (PEG) derivatives were obtained from Intezyne Technologies (Tampa, FL). ^{64}Cu was prepared on the Washington University Medical School CS-15 Cyclotron by ^{64}Ni(p,n)^{64}Cu nuclear reaction at a specific activity of 50−200 mCi/μg at the end of bombardment, as previously described.[22] The buffers used for ^{64}Cu-labeling were treated with Chelex-100 resin (Bio-Rad Laboratories, Hercules, CA) before use. Tris-*t*-butylester-DOTA was purchased from Macrocyclics (Dallas, TX). Centricon tubes (YM-30: molecular weight cutoff (MWCO) 30 kDa; YM-50: MWCO 50 kDa; YM-100: MWCO 100 kDa) were purchased from Millipore. HiTrap desalting columns (5 mL) were purchased from GE Healthcare Biosciences (Piscataway, NJ).

Polymeric materials were characterized by ^{1}H and ^{13}C nuclear magnetic resonance (NMR) spectroscopy using either a Bruker 200, 300, or 500 MHz spectrometer with the residual solvent signal as an internal reference. Gel permeation chromatography (GPC) was performed in tetrahydrofuran on a Waters system (Millford, MA) equipped with four 5 μm Waters columns (300 × 7.7 mm) connected in series with increasing pore size (10^2, 10^3, 10^4, and 10^6 Å). A Waters 410 differential refractometer index and 996 photodiode array detectors were employed. The molecular weights of the polymers were calculated relative to linear PS standards. Fourier transform infrared spectroscopy was performed using a Nicolet Magna 850 IR-Raman instrument on a CaF_2 salt plate. The spectra were acquired at 4 cm^{-1} resolution and 128 scans. A Bioscan 200 imaging scanner (Bioscan, Washington, D.C.) was used to read the instant thin layer chromatography (ITLC) plates (Pall ITLC-SG plates, VWR International, Batavia, IL). Fast protein liquid chromatography (FPLC) and radio-FPLC were performed using an ÄKTA FPLC system (GE Healthcare Biosciences) equipped with a Beckman 170 radioisotope detector (Beckman Instruments, Fullerton, CA). The dithioester RAFT agent, methacryloxysuccinimide (MASI), and tris-*t*-butyl-DOTA-amine were synthesized as reported elsewhere.[23−25]

Synthesis of Poly(ethylene glycol) Methyl Ether Methacrylate (PEGMA). Poly(ethylene glycol) monomethyl ether (mPEG, 5.0 kDa, 5.00 g, 1.00 mmol) was purified by column chromatography (Merck Kieselgel 60, 230−400 mesh) in dichloromethane/methanol (95:5), dried in vacuum, and dissolved in dichloromethane (25 mL) and triethylamine (5 mL). Freshly distilled methacryloyl chloride (5.00 mL, 5.35 g, 5.12 mmol) was added dropwise at 4 °C, and the reaction mixture was allowed to stir overnight under nitrogen. The reaction was quenched with water and filtered, and the organic phase was washed with 10% $NaHSO_4$ (w/v), dried over anhydrous $MgSO_4$, and concentrated in vacuum to approximately 10 mL. The product was precipitated by adding cold diethyl ether (200 mL) and drying in vacuum (4.65 g, 92%). ^{1}H NMR (200 MHz, $CDCl_3$) δ: 6.15 (1H), 5.58 (1H), 4.32 (2H), 3.6 (450H), 1.95 (2H). The 2 kDa PEGMA was synthesized similarly, whereas the 1.1 kDa PEGMA was purchased from Aldrich.

Synthesis of Comb Copolymers (1a−c). Comb copolymers were synthesized using standard RAFT conditions.[24,26] To illustrate, PEGMA 5.0 kDa (1.50 g, 0.300 mmol), methyl methacrylate (MMA, 239 mg, 2.39 mmol), azobisisobutyronitrile (AIBN, 0.222 mg, 1.35 μmol (as a 1 wt % DMF solution)), MASI (56.5 mg, 0.308 mmol), and RAFT agent (1.86 mg, 6.16 μmol (as a 1 wt % DMF solution)) were dissolved in DMF (2.37 mL). The solution was transferred to a sealing vial, and it underwent three freeze−pump−thaw cycles. The vial was then sealed under vacuum and heated at 70 °C for 24 h. Following polymerization, the solution was diluted with DMF, transferred to four 15 mL centricon tubes (YM-50), and extensively washed with DMF. The copolymer was then precipitated from the concentrated DMF solution (~5 mL) into cold diethyl ether (ca. 200 mL) and dried in vacuum to give the desired graft copolymer **1c** as a white solid (yield: 0.526 g, 35%). M_n = 91 800. Polydispersity index (PDI): 1.19. ^{1}H NMR (200 MHz, $CHCl_3$) δ: 0.75−1.85 (m, CH_2, CH, CH_3), 2.80−2.91 (br s, succinimide CH_2), 3.35−3.40 (OCH_3), 3.50−3.87 (s, −OCH_2CH_2O−), 4.08−4.35 (m, CO−CH_2CH_2O). FTIR (CaF_2): 2882, 1966, 1780, 1737, 1467, 1359, 1344, 1280, 1242, 1196, 1147, 1111, 1061 cm^{-1}.

In a similar fashion, the graft copolymer **1a** based on 1.1 kDa PEG was prepared from PEGMA 1.1 kDa (2.00 g, 1.82 mmol), methyl methacrylate (MMA, 545 mg, 5.45 mmol), azobisisobutyronitrile (AIBN, 0.60 mg, 3.65 μmol (as a 1 wt % DMF solution)), MASI (344 mg, 1.88 mmol), and RAFT agent (11.0 mg, 365 μmol (as a 1 wt % DMF solution)) dissolved in DMF (3.0 mL).

Using the same procedure, the graft copolymer **1b** based on 2.0 kDa PEG was prepared from PEGMA 2.0 kDa (1.00 g, 0.50 mmol), methyl methacrylate (MMA, 276 mg, 2.76 mmol), azobisisobutyronitrile (AIBN, 0.42 mg, 2.55 μmol (as a 1 wt % DMF solution)), MASI (90 mg, 0.49 mmol), and RAFT agent (3.74 mg, 124 μmol (as a 1 wt % DMF solution)) dissolved in DMF (1.25 mL).

Synthesis of 1,4,7,10-Tetraazacyclododecanetetraacetic Acid (DOTA)-Conjugated Comb Copolymers (2a−b). Copolymers **1a−c** were reacted with an excess of tris-*t*-butyl-DOTA-amine in DMF for 48 h at room temperature (RT) to afford copolymers **2a−c.** Representatively, **1c** (99.5 mg, 21 μmol NHS units) and tris-*t*-butyl-DOTA-amine (39.4 mg, 58.7 μmol) were stirred in DMF (2 mL) for 48 h at RT. The reaction mixture was then diluted with DMF (5 mL) and purified by centrifugal filtration (5 × 10 mL DMF). Final purification of the copolymers **2a−c** was by precipitation with cold diethyl ether (~50 mL) followed by drying in vacuum, and the yields of **2a−c** were 80−90%. Data for **2c** are as follows. M_n: 92 800. PDI: 1.22. ^{1}H NMR (200 MHz, $CHCl_3$) δ: 0.75−1.85 (m, CH_2, CH, CH_3), 1.41−1.47 (s, *t*-butyl), 2.62−2.72 (br s, succinimide CH_2), 3.35−3.40 (OCH_3), 3.50−3.87 (s, −OCH_2CH_2O−), 4.08−4.35 (m, CO−CH_2CH_2O).

DOTA Deprotection and Collapse of the Comb Copolymers. The *t*-butyl groups of the DOTA functional groups of the copolymers **2a−c** were deprotected with a 9:1 v/v mixture of dichloromethane/trifluoroacetic acid (TFA). Representatively, **2c** (10 mg) was dissolved in dichloromethane/TFA (9:1 v/v, 1 mL) and stirred overnight at RT. After solvent removal, the oily residue was redissolved in dichloromethane (1 mL) and precipitated in hexane (25 mL). This procedure was repeated three times followed by drying in vacuum. The obtained product was dissolved in dimethylsulfoxide (DMSO) (1% w/v), and then an equal volume of water was added in one aliquot to achieve collapse. The solution was stirred for 2−3 h, and DMSO was then eliminated by centrifugal filtration. After extensive washing, the nanoparticles were reconstituted in water (~3 mg/mL) and stored at 4 °C for further use.

Dynamic Light Scattering (DLS). DLS measurements were carried out on a Brookhaven BI-9000AT digital autocorrelator (Holtsville, NY) equipped with an Avalanche photodiode detector and a MG vertically polarized 35 mW He−Ne 633 nm laser and operated by the 9KDLSW control program. All samples were filtered through a 0.45 μm filter and then run in triplicate for 10 min at 25 °C, at 1 mg/mL, and at a fixed 90° angle. The hydrodynamic diameter and distribution of particles were determined by fitting the correlation functions with the ISDA analysis software package (Brookhaven Instruments Co.) and applying the non-negatively constrained least-squares particle size distribution analysis (NNLS).[27]

Cryogenic Transmission Electron Microscopy (Cryo-TEM). Sample preparation for cryo-TEM involved initial vitrification using an environmentally controlled, automated Vitrobot (FEI Company, Hillsboro, OR) system where a lacey carbon coated copper grid is

immersed into the polymer solution, blotted with filter paper, and plunged into liquid ethane. In a typical sample preparation, the chamber was maintained at 22 °C and 30−40% relative humidity, and the grid was immersed into a 0.1 wt % aqueous polymer solution for 5 s, blotted twice for 1 s each, and then plunged directly into liquid ethane. Once vitrified, the grids were transferred into liquid nitrogen and then into a cryo-holder (Gatan, Pleasanton, CA) before insertion into the electron microscope (precooled to −175 °C). Digital images were taken with a Tecnai G2 T12 Twin transmission electron microscope (FEI Company, Hillsboro, OR) operated at 120 kV using a charge-coupled device (CCD) camera (Gatan, Pleasanton, CA).

Small Angle Neutron Scattering (SANS). SANS experiments were performed on the 30 m instrument (NG-3)[28] at the NIST Center for Neutron Research (NCNR), National Institute of Standards and Technology (NIST), Gaithersburg, MD. A concentration of 0.1 wt % and a path length of 2 mm were used for all measurements. A monochromated neutron beam ($\lambda = 6$ Å) with a wavelength spread ($\Delta\lambda/\lambda$) of 0.14 was incident on the sample. The scattered neutrons were captured on a 64 cm × 64 cm 2-D detector. Varying sample-to-detector distances of 1.33, 4.5, and 13.17 m were used to study the scattering wave vector q in the range $0.004 < q$ (Å^{-1}) < 0.1, defined by $q = (4/\lambda)\sin(\theta/2)$, where λ is the neutron wavelength and θ is the scattering angle. The raw data were corrected for background electronic noise and radiation, detector inhomogeneity and sensitivity, and empty cell scattering. Intensities were normalized to an absolute scale relative to the main beam transmission measurements through the sample and were reduced according to a published protocol.[29] The data were fit using a smeared polydisperse core and shell model[30] with a hard sphere structure factor, in which the shell thickness is maintained constant. Such a model closely approximates the micelles in solution, as the hydrophobic PMMA core is densely packed, while the hydrophilic PEG chains are fully solvated in the good solvent (D_2O).

Radiolabeling of DOTA-Nanoparticles with ^{64}Cu. ^{64}Cu-chloride (5−10 μL in 0.5 M HCl) was diluted with 0.1 M ammonium acetate buffer (pH 7.0, 50−100 μL). The nanoparticle solutions (1 mg/mL, 30−200 μL) were 2-fold diluted with acetate buffer, ^{64}Cu-acetate (2−5 mCi) was added, and the mixture was incubated at 80 °C for 1 h. Following this, 5−10 μL of an aqueous diethylenetriaminepentaacetic acid (DTPA) solution was added and incubation continued for 10 min at room temperature (RT). HiTrap desalting columns were used to separate the radiolabeled products from the residual free ^{64}Cu and/or ^{64}Cu-DTPA complex. The labeling yield was determined by radio-ITLC using a 1:1 mixture (v/v) of 10 wt % ammonium acetate and methanol as eluent. After purification, the radiochemical purity (RCP) of the ^{64}Cu-labeled nanoparticles was monitored by radio-FPLC. The products were then diluted with 10 mM phosphate-buffered saline (PBS, pH 7.4) to prepare appropriate doses for biodistribution and imaging studies.

The *in vitro* stability of the ^{64}Cu-labeled nanoparticles was evaluated by incubating the compounds in both PBS and mouse serum (Sigma-Aldrich) and by analyzing aliquots by radio-ITLC at different time points up to 48 h.

The number of DOTA groups attached to the copolymers was estimated by adding 100 μg of the nanoparticles to a known excess of "hot plus cold" Cu-acetate (a nonradioactive Cu-acetate solution spiked with 50−100 μCi ^{64}Cu). After 2 h incubation at 80 °C, DTPA was added and the resulting solution was incubated for 10 min at RT. Aliquots (2 μL) were then analyzed by radio-ITLC: the Cu-labeled nanoparticles remained at the origin, while the Cu-DTPA complex migrated with an R_f of 0.9. The number of DOTA chelates attached to the comb copolymers was determined from the counts per minute (cpm) in the radio-chromatogram, with the following equation:

$$n(\text{chelates}) = \frac{n(\text{copper}) \times \text{cpm}(R_f < 0.3)}{\text{cpm(total)}}$$

FPLC Analysis. A 100 μL analyte of the labeled nanoparticle was injected into a Superose 12 gel filtration column (GE Healthcare Biosciences) and eluted with 20 mM Hepes and 150 mM NaCl (pH 7.3) at 0.8 mL/min. The UV wavelength was preset to 280 nm, and the radioactivity was monitored by an in-line radio-detector. Under these conditions, the retention times of the native and radiolabeled nanoparticles were 10−18 min while the retention times of free ^{64}Cu and ^{64}Cu-DTPA were 20−22 min. Samples with RCP > 95% were used for animal studies.

Biodistribution Studies. All animal studies were performed in compliance with guidelines set by the Washington University Animal Studies Committee. Normal female Sprague−Dawley rats (180−200 g, $n = 3-4$ per time point) were anesthetized with 1−2% vaporized isoflurane and injected with approximately 30 μCi/200 μL of activity via the tail vein (∼80−100 μg/kg rat body weight). The rats were anesthetized prior to sacrifice at each time point. Organs and tissues of interest were removed and blotted dry, and the radioactivity was measured in a gamma counter. The total activity in the blood was calculated assuming 6% of the rat body weight. Diluted standard doses (1:100) were prepared and counted along with the samples. All the data were corrected for ^{64}Cu decay. The percent injected dose per gram of tissue (%ID/g) values were calculated using the following equation:

$$\%\text{ID/g} = \frac{(\text{cpm in sample} - \text{background}) \times 10^2}{(\text{decay correction factor}) \times (\text{sample weight}) \times (\text{cpm in standard})}$$

One-way analysis of variance (ANOVA) and post-hoc multiple comparison (Bonferroni's *t*-test) on the biodistribution data were performed using Prism version 4.00 (GraphPad, San Diego, CA).

Small Animal Positron Emission Tomography (PET) Imaging Studies. The imaging studies were carried out using the MicroPET Focus (CTI-Concorde Microsystems, Knoxville, TN) and the MicroCAT II (CTI-Imtek, Knoxville, TN) scanners. Normal BALB/c mice weighing 20−30 g were injected with ∼100−200 μCi of ^{64}Cu-labeled particles (1.5−2 mg/kg body weight) in 150 μL saline via the tail vein and anesthetized with 1−2% vaporized isoflurane for data collection at specific time points. MicroPET and microCT image coregistration was accomplished using a landmark registration technique (by using fiducial markers directly attached to the animal bed) and AMIRA image display software (AMIRA, TGS Inc., Richmond, TX). Data analysis of microPET images was performed using the manufacturer software (ASIPRO, CTI-Concorde MicroSystem). Data were calculated in terms of standardized uptake values (SUVs) in 3-D regions of interest (ROIs) using the following equation:

$$\text{SUV} = \frac{\text{radioactivity concentration in ROI [}\mu\text{Ci/cc]}}{\text{injected dose [}\mu\text{Ci]/animal weight [g]}}$$

Results and Discussion

Synthesis of Comb Copolymers. In designing a synthetic strategy for the preparation of polymeric nanoparticles suitable for diagnostic and biodistribution studies, it was decided initially that the diagnostic tool of choice was positron emission tomography due to its high resolution and wide applicability. Previously, ^{64}Cu has been shown to be a very effective radiolabel for assessing the behavior of nanomaterials *in vivo*,[31−33] with favorable decay characteristics, and ^{64}Cu (β^+: 0.653 MeV, 17.4%; β^-: 0.578 MeV, 39%) is currently being investigated for both radiotherapy and positron emission tomography (PET) in humans.[34] Furthermore, the half-life of ^{64}Cu (12.7 h) allows the tracking of radiolabeled materials *in vivo* for prolonged times. For the controlled incorporation of ^{64}Cu, highly efficient binding ligands such as the 1,4,7,10-tetraazacyclododecanetetraacetic acid (DOTA) ligand were chosen and orthogonal amidation chemistry via active ester groups was selected for the coupling reaction.

Scheme 1

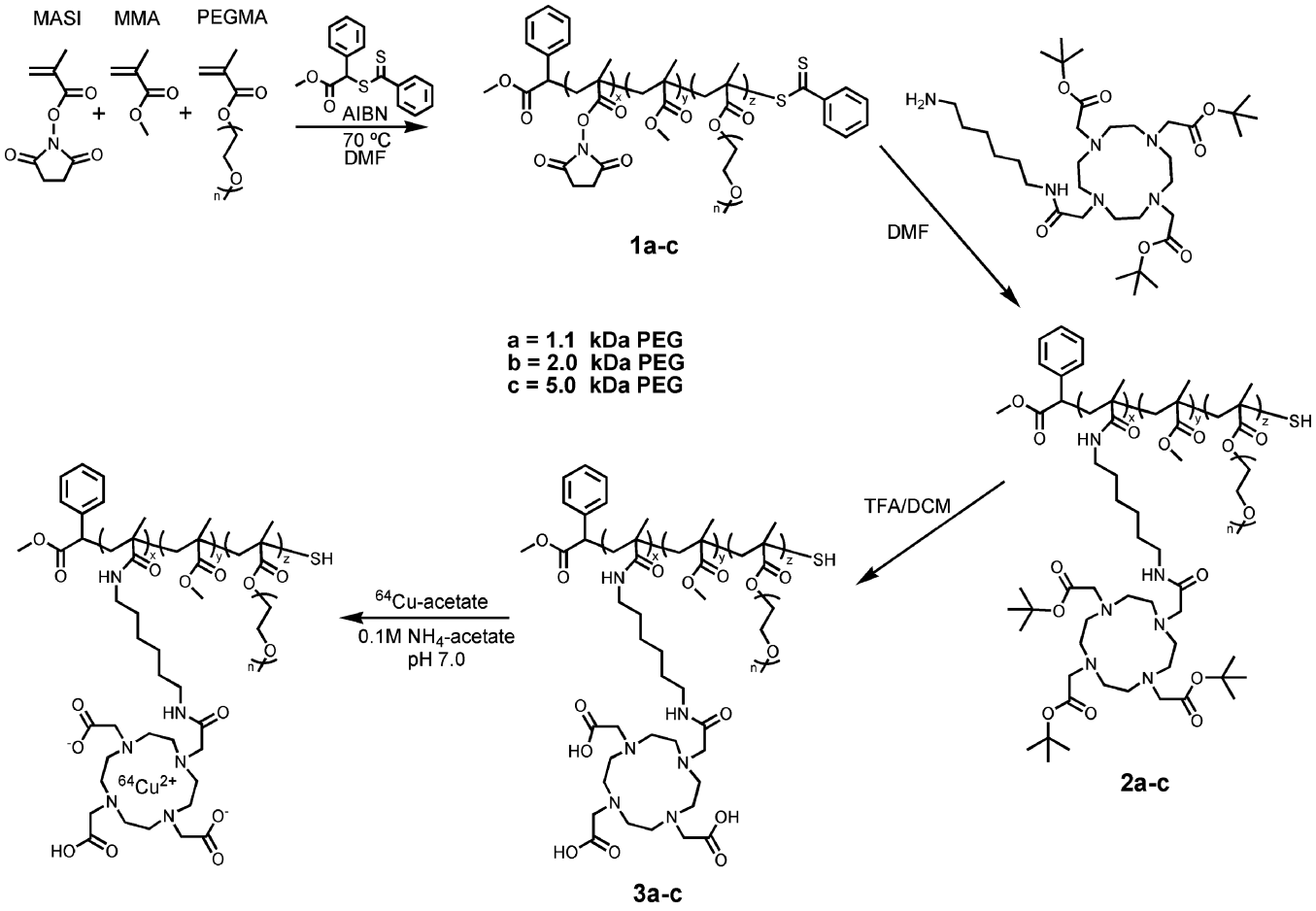

The mild reaction conditions and absence of metal ion catalysts for reversible addition fragmentation transfer (RAFT) polymerization in contrast to nitroxide mediated[35] or atom transfer radical[36] techniques defined the synthetic strategy as shown in Scheme 1. Terpolymerization of methyl methacrylate (MMA), the active ester monomer, methacryloxysuccinimide (MASI), and poly(ethylene glycol)monomethacrylate (PEGMA) in the presence of the dithioester RAFT agent was shown to be a living process leading to low polydispersity comb polymers with control over the molecular weight of the backbone polymer as well as the percent incorporation of each repeat unit.[44] By incorporating PEG chains, the comb copolymer is amphiphilic and undergoes collapse in aqueous solution, leading to the formation of a nanoparticle in which the PEG chains form an external corona surrounding the hydrophobic methacrylate backbone in the interior. In addition, the length of the grafted PEG arms can be varied by using different PEGMA macromonomers (1.1, 2.0, and 5.0 kDa) in the initial monomer feed. This control allows a library of polymers and associated nanoparticles to be prepared, which is critical for developing structure/property relationships to determine the effects of molecular structure on biological performance. Finally, the level of incorporation of the active ester repeat units and, after attachment of tris-*t*-butyl-DOTA-amine, the ^{64}Cu chelating units could be quantified before formation of the nanoparticle (Table 1).[25] For example, comb polymers were prepared with an overall number of backbone repeat units of 80−160 which correlates with approximately 20−25 PEG chains per comb and approximately 20−25 active sites (NHS groups) for DOTA attachment per macromolecule. Purification of the PEG-comb polymers was accomplished by centrifugal filtration using 30 000 and 50 000 Da cutoff membranes and was shown to efficiently remove any unreacted PEG-macromonomer. Reaction of tris-*t*-butyl-DOTA-amine with the NHS esters along the copolymer backbone allowed conjugation of DOTA ligands to the comb structure, and ^{1}H NMR spectroscopy was used to confirm attachment of DOTA (appearance of *t*-butyl protons at 1.5 ppm, Figure 1b) and quantify the level of DOTA incorporation (Scheme 1).[38]

Table 1. Structural Features of DOTA-Functionalized Graft Copolymers, **3a**−**c**

polymer	PEG graft	%PEG (wt %)	M_n (GPC)	PDI (GPC)	D_h (DLS)[a]
3a	1.1 kDa	66	26 000 Da	1.3	9.7 ± 1.1 nm
3b	2.0 kDa	72	60 300 Da	1.3	17 ± 2 nm
3c	5.0 kDa	82	91 800 Da	1.3	20 ± 3 nm

[a] Size measured after copolymer collapse and nanoparticle assembly in water.

Nanoparticle Formation. In analogy with more traditional linear, amphiphilic diblock copolymers,[13,14] the comb copolymers do not readily dissolve into water to form nanoparticles, presumably due to their comb architecture and associated hydrophobic PMMA backbone. To afford water dispersed nanoscale assemblies of the amphiphilic block graft copolymer materials, the copolymers were dissolved initially into DMSO, water was added, and the DMSO was removed by membrane filtration/dialysis to afford stable and well-defined nanoparticles as confirmed by DLS (Table 1). The hydrodynamic diameters of the collapsed nanoparticles ranged from 10 to 20 nm (Table 1), and this increase in nanoparticle size is fully consistent with the increase of the molecular weight of the PEG grafts.

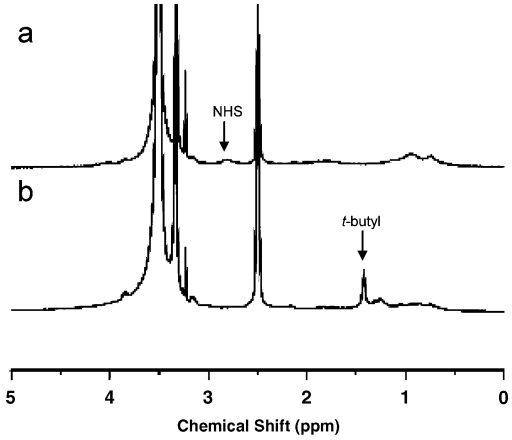

Figure 1. H NMR analysis showing the attachment of DOTA to 2.0 kDa comblike copolymers (a) before reaction where NHS groups are visible and (b) after attachment showing the appearance of the *t*-butyl peaks from DOTA.

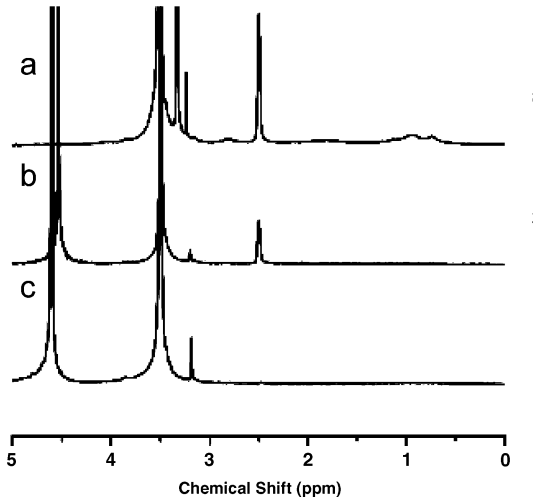

Figure 2. H NMR analysis of the assembly process for the 2.0 kDa comblike copolymer, **3b**, in (a) DMSO-d_6 , (b) 1:1 (vol) DMSO-d_6/D_2O, and (c) D_2O showing the decrease in solvation of the PMMA backbone as it forms the nanoparticle core.

To study the formation of the core−shell nanoparticles by collapse of the comblike copolymers further, NMR studies were carried out in deuterated solvent throughout the self-assembly process for the deprotected copolymers derived from the 2.0 kDa PEG macromonomer, **3b** (Figure 2). Both the PEG peaks (backbone CH_2 groups at 3.5 ppm and terminal OCH_3 group at 3.2 ppm) and the PMMA backbone peaks (1.8 and 0.8 ppm) are clearly visible in the NMR spectrum of the extended polymer in DMSO (Figure 2a). Upon addition of D_2O, all of the characteristic PMMA peaks become attenuated as the mobility of the backbone decreases significantly on forming the nonsolvated hydrophobic core of the polymer nanoparticle. Following complete DMSO removal, only the PEG peaks are visible in the NMR spectrum (Figure 2c). To confirm the low polydispersity and core−shell morphology of these nanoparticles, aqueous cryo-TEM experiments were conducted on all samples, and, in each case, well-defined nanoparticles were observed. For example, TEM measurements clearly show that the deprotected nanoparticles obtained from the 5 kDa PEG comb copolymer, **3c**, had diameters of the collapsed PMMA core (11.6 ± 3.9 nm) with a well-resolved and solvated PEG corona (Figure 3). In addition, the size of the overall nanoparticles from TEM (21.8 ± 3.2 nm) agrees well with the hydrodynamic diameters obtained from DLS (20 ± 3 nm). Finally, small angle

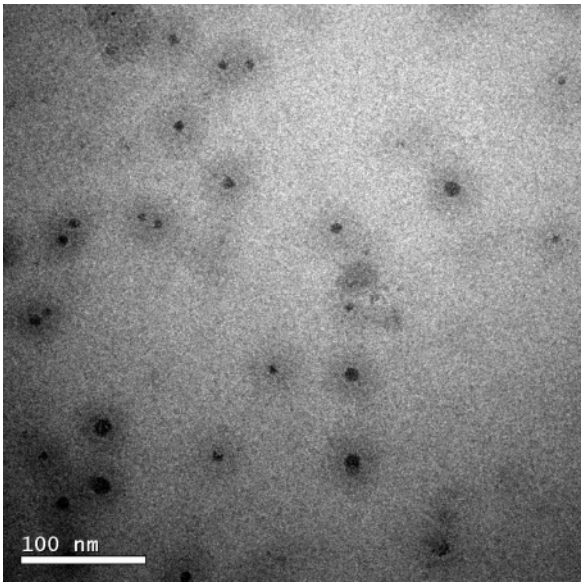

Figure 3. Cryo-TEM image of the 5.0 kDa PEG nanoparticle, **3c**, showing core−shell morphology.

neutron scattering (SANS) of the 5 kDa PEG derived nanoparticle, **3c**, was performed to further elucidate the core−shell morphology, and the model fitting gives a core radius of 3.9 nm and a shell thickness of 2.5 nm. Thus, the average micelle diameter, obtained from this global analysis, is 12.8 nm. A Guinier analysis of the data in the low q saturation regime gives a micelle radius of 7.0 ± 0.2 Å (Figure 4).

^{64}Cu-Radiolabeling of DOTA-Conjugated Nanoparticles. ^{64}Cu-radiolabeling was accomplished by initially deprotecting the *t*-butyl esters of the DOTA groups with trifluoroacetic acid (which did not degrade other esters) followed by incubating the DOTA-conjugated nanoparticles with ^{64}Cu in acetate buffer. Radiolabeling in pH 7.0 acetate buffer was found to be similar to that in pH 8.0 buffer and much improved over other conditions tested (DMSO, 50:50 DMSO/H_2O, and lower pH buffers). Nonspecific binding of ^{64}Cu to amide and ester functionalities within the particle core was overcome by adding a linear, small molecule chelating agent, DTPA, to the labeling mixture, followed by centricon separation.[34] This DTPA challenge procedure successfully removed weakly bound ^{64}Cu, ensuring that all of the remaining ^{64}Cu was coordinated specifically and stably within the DOTA macrocycles conjugated to the nanoparticles. All of the ^{64}Cu-labeled nanoparticles showed greater than 95% RCP following DTPA challenge and size exclusion purification, as determined by radio-FPLC. The number of conjugated DOTA ligands available to interact with ^{64}Cu was determined to be 0.5 per 1 kDa PEG comb, 0.7 per 2 kDa PEG comb, and 3.0 per 5 kDa PEG comb (~3, 5, and 21 per respective particle) through a modified isotopic dilution assay.[32] The estimated number of DOTA groups was found to be lower than that obtained by ^{1}H NMR spectroscopy, presumably due to incomplete penetration of ^{64}Cu within the hydrophobic core of the nanoparticles in aqueous solution. Though the reactivity of DOTA functionalities was only partial, the obtained specific activity (10−20 μCi/μg) was suitable for *in vivo* evaluation of the nanoparticles. The nanoparticles exhibited prolonged *in vitro* stability (>80% after 48 h incubation at 37 °C) in both PBS and mouse serum, as confirmed by radio-ITLC.

Biodistribution Studies. The influence of macromolecular architecture and structure on biodistribution and blood circulation lifetimes was evaluated by examining the performance of nanoparticles derived from three different PEG molecular weight

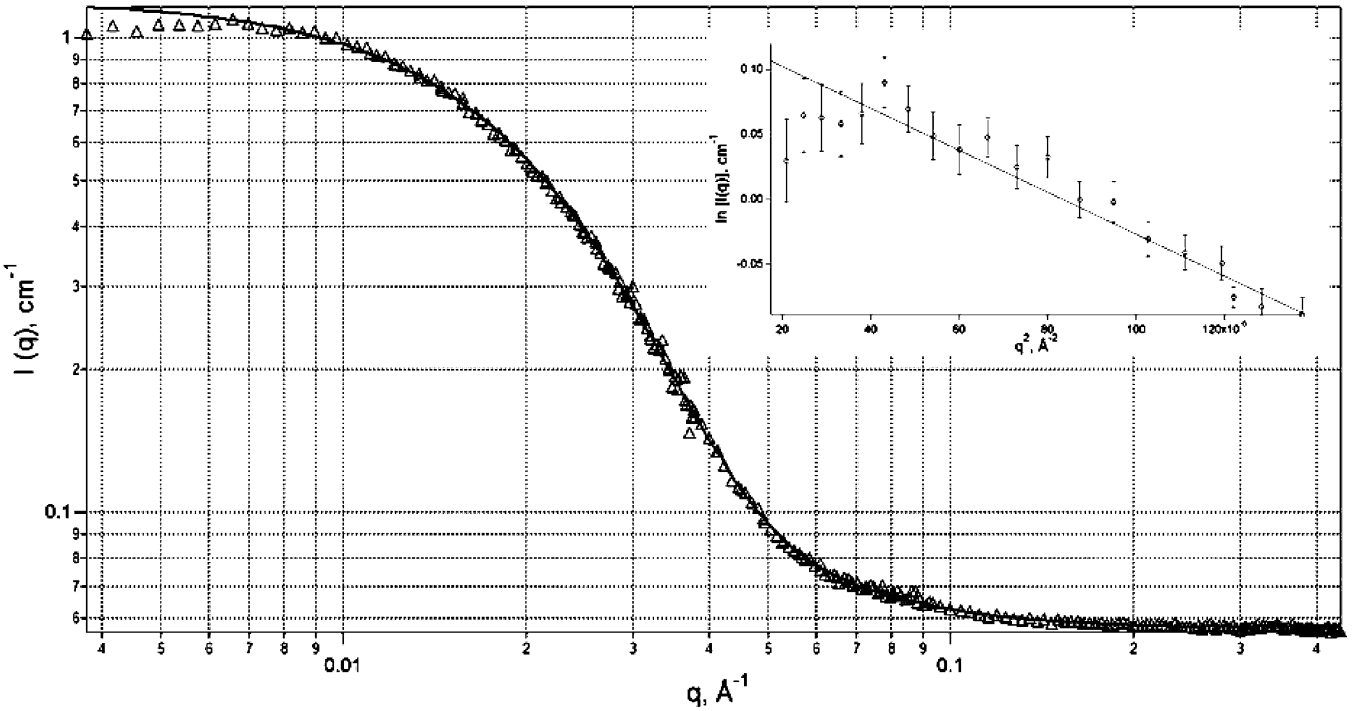

Figure 4. SANS data from 0.1 wt % **3c** solution in D_2O. The solid line is a polydisperse core and shell form fit with a hard sphere structure factor. The error bars of the data points are within the limits of the symbols. Inset: Guinier plot ln[$I(q)$] versus q^2 for low q data.

macromonomers (1.1, 2.0, and 5.0 kDa). To this aim, ^{64}Cu-labeled nanoparticles were administered intravenously (iv) to normal rodents and blood retention, accumulation in the main organs (liver, spleen, kidney, and lungs), and excretion through urine and feces were studied in detail.

All three PEG nanoparticles exhibited high blood retention shortly after administration (Figure 5a) which is significantly longer than the ^{64}Cu-DOTA small molecule complex which is excreted through the kidneys within minutes.[39] However, the 1.1 kDa PEG nanoparticle showed a fast blood clearance, with considerably lower blood levels than the 2.0 kDa and 5.0 kDa PEG nanoparticles at each considered time point. Significantly, 60−65% of the administered 5.0 kDa and 2.0 kDa PEG nanoparticle derivatives remained in the blood for at least 4 h after iv administration, while only 27 ± 2 % of the 1.1 kDa PEG nanoparticle was still in the blood at the same time point. Thereafter, the 5.0 kDa PEG nanoparticle underwent a slow clearance, with 31 ± 2% of the dose still in the blood at 48 h postinjection (p.i.) (10-fold higher than that of the 1.1 kDa PEG nanoparticle). Of particular note is that the intermediate structure derived from 2.0 kDa PEG macromonomers exhibited features of both the corresponding high and low molecular weight analogues. The blood level was similar to that of the 5.0 kDa PEG nanoparticle up to 4 h p.i., and then the blood clearance profile changed and began to resemble that of the 1.1 kDa PEG nanoparticle out to 48 h p.i. This demonstrates that the blood circulation lifetimes of polymeric nanoparticles can be manipulated based on the macromolecular architecture and synthetic design.

A classical problem with prior *in vivo* nanoparticle strategies has been nanoparticle accumulation in the liver. This behavior is understandable, as the liver contains principal phagocytic cells (Kupffer cells, hepatocytes, hepatic stellate cells, etc.) and is one of the main organs, along with the spleen and bone marrow, which eliminates foreign particulates, macromolecules, and senescent cells.[40] In examining the liver burden profile for the tailored PEG nanoparticles, a similar strong correlation between structure and performance was observed. In this case, the biodistribution trend in the liver was opposite to that observed in the blood with the hepatic accumulation of 1.1 kDa PEG nanoparticles being significantly higher than that of the other two higher molecular weight PEG analogues up to 24 h p.i. (Figure 5b). A considerable nanoparticle uptake in the first few hours p.i. was observed for the 1.1 kDa derivative followed by a slow release, whereas the hepatic uptake of the larger nanoparticles was less marked and no significant differences were observed between the 2.0 kDa and 5.0 kDa PEG nanoparticle analogues until 4 h p.i.. At later time points, the hepatic accumulation of the 2.0 kDa PEG nanoparticle began to increase while the uptake of the 5.0 kDa PEG nanoparticle stabilized.

The biodistribution data relative to the spleen are shown in Figure 5c. Contrary to the liver, no significant differences were observed between the splenic uptakes of the two smaller particles while the accumulation of the 5.0 kDa PEG nanoparticle was the lowest immediately after administration and increased over time when compared to those of the other two polymers. Based on previously reported findings, this uptake of the 5.0 kDa PEG nanoparticle may be due to the larger hydrodynamic diameter with respect to other evaluated nanoparticles.[2]

The uptake of the three evaluated nanoparticles in the lung (Figure 5d) was moderate, and it has a pattern resembling that observed in the blood. This finding suggests the presence of some residual blood in the harvested organs (blotted dry but not perfused before counting), more so than a tissue specific particle distribution. However, the absence of relevant amounts of radioactivity in this organ is an indirect sign of the stability of the nanoparticle preparations. In fact, *in vivo* nanoparticle aggregation would lead to significant accumulation of radioactivity levels in the lung,[32] which is the first capillary bed that materials encounter upon tail vein injection.

In terms of excretion, the 1.1 kDa PEG nanoparticle exhibited a significantly higher urinary load compared to the 5.0 kDa PEG derivative (Table 2, $P < 0.01$) as confirmed also by the kidney distribution data (Figure 5e). These findings are reasonable, as the molecular weight cutoffs for glomerular filtration of native globular proteins and linear PEG are considered to be ap-

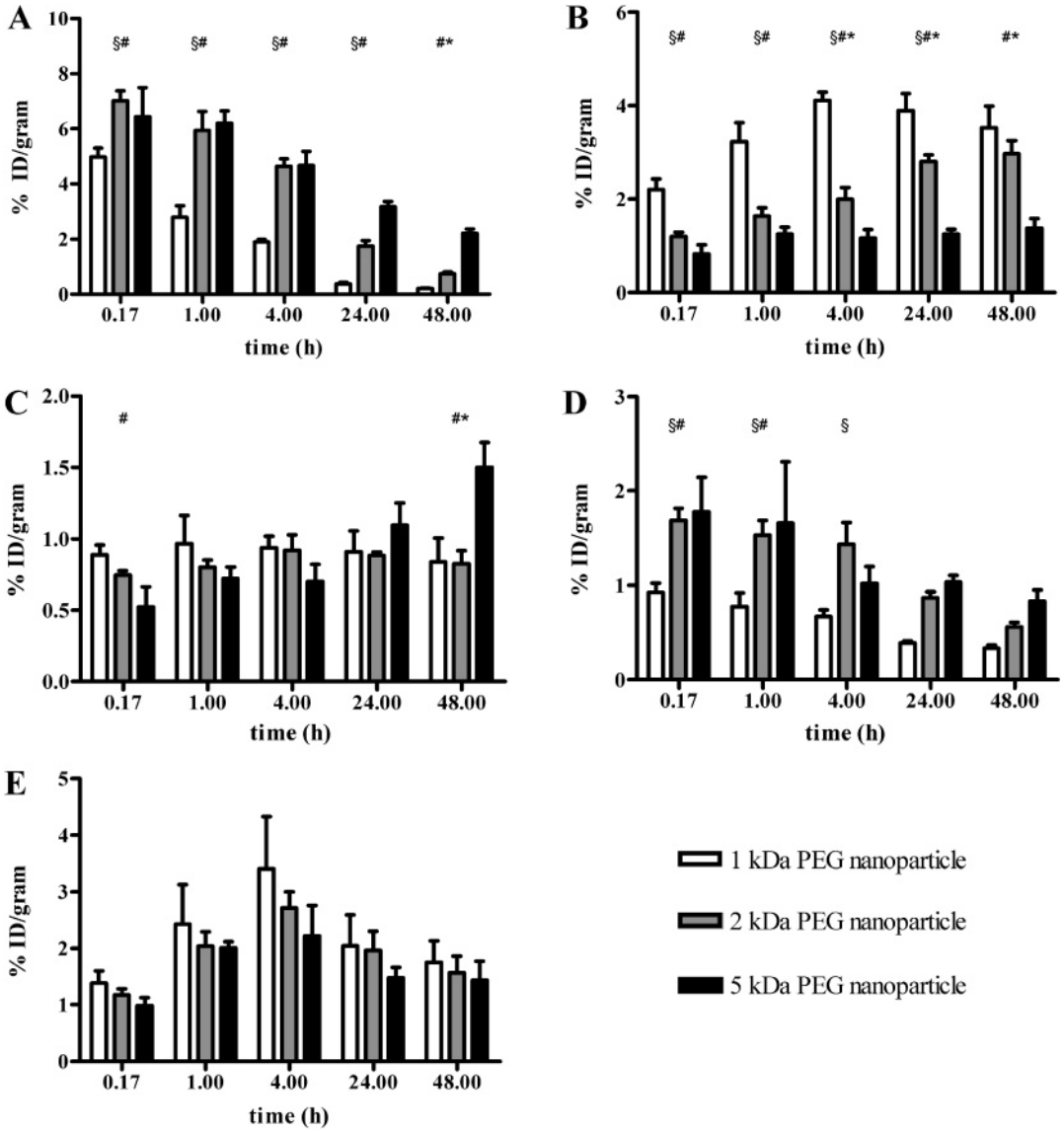

Figure 5. Biodistribution data for the ^{64}Cu-labeled particles in Sprague−Dawley rats ($n = 3-4$; ~80 μg/kg rat; ANOVA: $P < 0.0001$). Data are expressed as percent injected dose per gram (%ID/g) ± SD. (A) Blood; (B) liver; (C) spleen; (D) lung; and (E) kidney (§: $P < 0.01$ for 1 kDa compared with that for 2 kDa PEG nanoparticles; #: $P < 0.01$ for 1 kDa compared with that for 5 kDa PEG nanoparticles; *: $P < 0.01$ for 2 kDa compared with that for 5 kDa PEG nanoparticles).

Table 2. Excretion Profiles for ^{64}Cu-Labeled Nanoparticles at Various Times Postinjection in Sprague−Dawley Rats ($n = 4$; 80−100 μg/kg Rat Weight)[a]

	urine			feces		
nanoparticle	4 h	24 h	48 h	4 h	24 h	48 h
1c	1.8 ± 0.3	8.7 ± 1.4	12.5 ± 1.5	0.0 ± 0.0	5.2 ± 2.7	11.8 ± 5.2
2c	2.8 ± 0.6	7.9 ± 0.4	10.4 ± 0.6	0.0 ± 0.0	5.5 ± 1.4	12.4 ± 1.2
3c	NA	5.1 ± 0.7	8.1 ± 1.1	NA	4.1 ± 0.8	8.8 ± 1.7

[a] Data expressed as percent injected dose ± SD. NA: not applicable.

proximately 70 and 30 kDa, respectively,[9] and the pore size of the glomerular basement membrane is in the range of 3−5 nm.[41] However, despite large hydrodynamic sizes, the renal filtration of highly flexible linear polymers is a known phenomenon (end-on "reptation").[9,42] These nanoparticles appear to allow slow renal filtration in a size-dependent fashion (1.1 kDa PEG nanoparticles >2.0 kDa PEG nanoparticles >5.0 kDa PEG nanoparticles), even though the particles are larger than the reported glomerular pore size (Table 2). It is important to note that the sizes of the individual graft copolymer components that constitute the larger nanoparticulate assemblies are expected to possess hydrodynamic diameters that are approximately 25% the size of the fully assembled aggregate, so that renal excretion may be provided by a dynamic disassembly/reassembly/reorganization of the supramolecular nanoassemblies.

Small Animal Imaging Studies. Having demonstrated a distinct correlation between nanoparticle structure and biodistribution combined with very promising blood circulation lifetimes for the 5.0 kDa PEG derivatives, small animal imaging studies were carried out in BALB/c mice. The coregistered microPET/microCT images (Figure 6) and the quantitative analyses obtained from microPET images (Figure 6) show

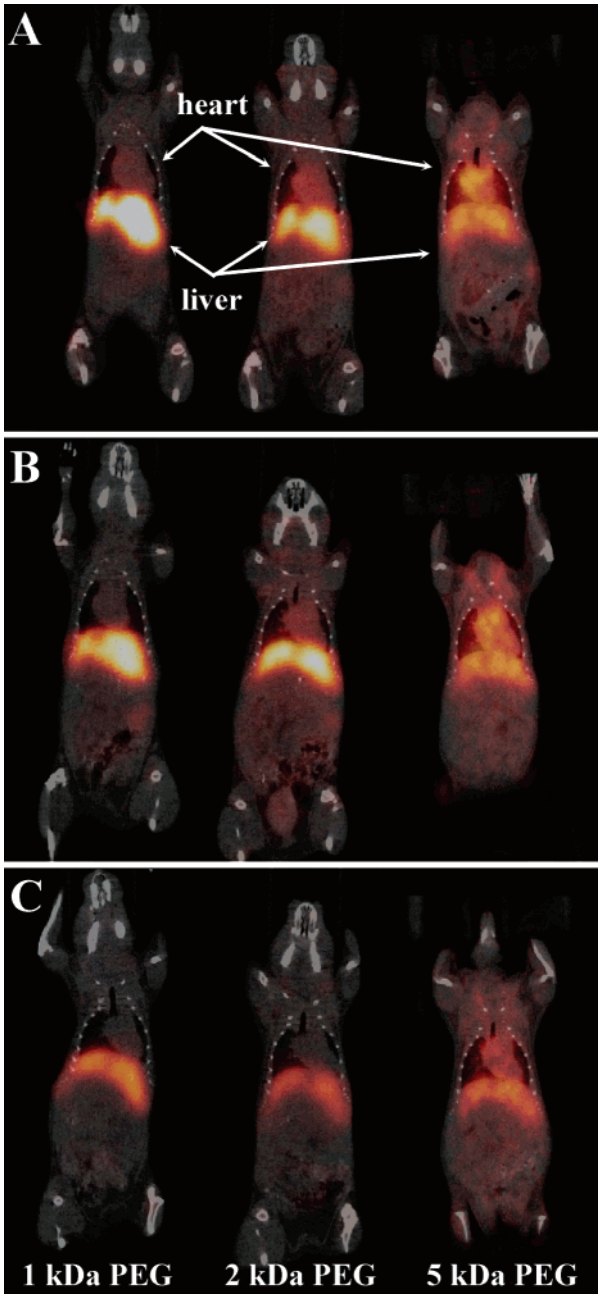

Figure 6. MicroPET/microCT images (decay corrected and scaled by min max frame) obtained by administering ^{64}Cu-labeled nanoparticles in BALB/c mice (~1.5−2 mg/kg mouse body weight): (a) 1 h postinjection (p.i.); (b) 4 h p.i.; and (c) 24 h p.i. (Left) 1.1 kDa PEG nanoparticle, **1c**; (center) 2.0 kDa PEG nanoparticle, **2c**; and (right) 5.0 kDa PEG nanoparticle, **3c**.

general concordance with the biodistribution studies. Following administration of the 5.0 kDa PEG-based nanoparticle, the mice hearts were clearly imaged out to 24 h p.i., confirming the presence of the nanoparticles in the bloodstream. On the contrary, the accumulation of 1.1 kDa PEG derived nanoparticles was prominent and persistent within the liver out to 24 h p.i., while little uptake was observed in the heart after 1 h p.i. As observed previously, the 2.0 kDa PEG nanoparticle exhibited an intermediate behavior between the 1.1 kDa and the 5.0 kDa PEG nanoparticles, and it is interesting to note that the blood circulation and liver accumulation trends are seen in both mice and rats and again can be correlated to the molecular structure of the nanoparticles (Figure 7).

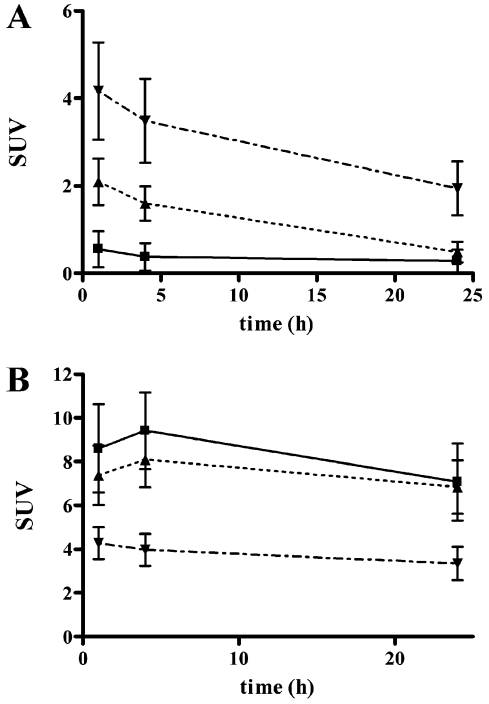

Figure 7. Comparative (A) heart and (B) lung standard uptake values (SUVs) for the ^{64}Cu-radiolabeled nanoparticles from the quantitation of microPET images in BALB/c mice ($n = 2-3$). Data are obtained from 3-D regions of interest and presented as mean SUV ± SD. (■) 1.1 kDa PEG nanoparticle, **3a**; (▲) 2.0 kDa PEG nanoparticle, **3b**; and (▼) 5.0 kDa PEG nanoparticle, **3c**.

Conclusions

A new class of core−shell nanoparticles have been synthesized via the controlled collapse of well-defined comb copolymers containing a hydrophobic PMMA backbone, water-soluble poly(ethylene glycol) grafted chains, as well as active ester groups that allow the attachment of functional moieties. Different facets of the nanoparticle structure could be controlled by varying the molecular parameters of these units, with the size of the nanoparticle corona being controlled by the molecular weight of the PEG graft. The presence of active functionalities on the copolymer backbone allowed the covalent attachment of DOTA ligands for the stable chelation of ^{64}Cu within the nanoparticle core. Biodistribution and small animal PET imaging studies in normal rodents demonstrated a strong correlation between the structure of the nanoparticles and their biological performance, with the molecular weight of the PEG grafts greatly influencing the circulation and organ uptake of these nanoparticles *in vivo*. A trend emerged that correlates longer PEG lengths with longer blood circulation lifetimes and lower uptake in the liver, showing the impact of a molecular parameter on biological activity. This is an important and fundamental step toward the development of smart nanomaterials for drug delivery and imaging of disease states, and it demonstrates an important synergy between the correct design of molecular parameters and synthetic strategy with accurate control over blood retention, MPS uptake, and excretion. Moreover, the dynamic nature of the supramolecular nanoassemblies suggests opportunities for tuning the biological behavior to be dependent on both the structure and composition of the polymer component, as well as the full nanoscale assembly. Investigations of the stability of these nanoassemblies and the ability of these materials to serve as hosts for the packaging and controlled release of guests, as a function of changing environments and

physical stimuli, such as those that may be encountered within different biological/organ spaces, are underway.

Acknowledgment. We thank Nicole Fettig, Margaret Morris, Dawn Werner, Lori Strong, Ann Stroncek, and Terry Sharp for technical assistance in the biodistribution and imaging studies. This material is based upon work supported by the National Institutes of Health as a Program of Excellence in Nanotechnology (HL080729). This work was partially supported by the MRSEC Program of the National Science Foundation (DMR05-20415). The production of ^{64}Cu is supported by a grant from the National Cancer Institute (CA86307).

References and Notes

(1) Wagner, V.; Dullaart, A.; Bock, A. K.; Zweck, A. *Nat. Biotechnol.* **2006**, *24*, 1211−1217.
(2) Chen, J.; Corbin, I. R.; Li, H.; Cao, W.; Glickson, J. D.; Zheng, G. *J. Am. Chem. Soc.* **2007**, *129*, 5798−5799. Rieter, W. J.; Kim, J. S.; Taylor, K. M. L.; An, H.; Lin, W.; Tarrant, T.; Lin, W. *Angew. Chem., Int. Ed.* **2007**, *46*, 3680−3682.
(3) Drummond, D. C.; Meyer, O.; Hong, K. L.; Kirpotin, D. B.; Papahadjopoulos, D. *Pharmacol. Rev.* **1999**, *51*, 691−743. Moghimi, S. M.; Hunter, A. C.; Murray, J. C. *Pharmacol. Rev.* **2001**, *53*, 283−318.
(4) Owens, D. E., III; Peppas, N. A. *Int. J. Pharm.* **2006**, *307*, 93−102.
(5) Vonarbourg, A.; Passirani, C.; Saulnier, P.; Benoit, J. P. *Biomaterials* **2006**, *27*, 4356−4373.
(6) Gref, R.; Luck, M.; Quellec, P.; Marchand, M.; Dellacherie, E.; Harnisch, S.; Blunk, T.; Muller, R. H. *Colloids Surf., B* **2000**, *18*, 301−313.
(7) Zahr, A. S.; Davis, C. A.; Pishko, M. V. *Langmuir* **2006**, *22*, 8178−8185.
(8) Vonarbourg, A.; Passirani, C.; Saulnier, P.; Simard, P.; Leroux, J. C.; Benoit, J. P. *J. Biomed. Mater. Res. A* **2006**, *78A*, 620−628.
(9) Caliceti, P.; Veronese, F. M. *Adv. Drug Delivery Rev.* **2003**, *55*, 1261−1277.
(10) Moghimi, S. M.; Szebeni, J. *Prog. Lipid Res.* **2003**, *42*, 463−478.
(11) Mosqueira, V. C. F.; Legrand, P.; Gulik, A.; Bourdon, O.; Gref, R.; Labarre, D.; Barratt, G. *Biomaterials* **2001**, *22*, 2967−2979.
(12) Mosqueira, V. C. F.; Legrand, P.; Morgat, J.-L.; Vert, M.; Mysiakine, E.; Gref, R.; Devissaguet, J. P.; Barratt, G. *Pharm. Res.* **2001**, *V18*, 1411−1419.
(13) Dunn, S. E.; Brindley, A.; Davis, S. S.; Davies, M. C.; Illum, L. *Pharm. Res.* **1994**, *V11*, 1016−1022.
(14) Limer, A. J.; Rullay, A. K.; San Miguel, V.; Peinado, C.; Keely, S.; Fitzpatrick, E.; Carrington, S. D.; Brayden, D.; Haddleton, D. M. *React. Funct. Polym.* **2006**, *66*, 51−64.
(15) Mantovani, G.; Lecolley, F.; Tao, L.; Haddleton, D. M.; Clerx, J.; Cornelissen, J.; Velonia, K. *J. Am. Chem. Soc.* **2005**, *127*, 2966−2973.
(16) Nicolas, J.; San Miguel, V.; Mantovani, G.; Haddleton, D. M. *Chem. Commun.* **2006**, 4697−4699.
(17) Kataoka, K.; Harada, A.; Nagasaki, Y. *Adv. Drug Delivery Rev.* **2001**, *47*, 113−131.
(18) Torchilin, V. P. *J. Controlled Release* **2001**, *73*, 137−172.
(19) Wooley, K. L. *J. Polym. Sci., Part A: Polym. Chem.* **2000**, *38*, 1397−1407.
(20) Murthy, K. S.; Ma, Q. G.; Clark, C. G.; Remsen, E. E.; Wooley, K. L. *Chem. Commun.* **2001**, 773−774.
(21) Xu, P. S.; Tang, H. D.; Li, S. Y.; Ren, J.; Van Kirk, E.; Murdoch, W. J.; Radosz, M.; Shen, Y. Q. *Biomacromolecules* **2004**, *5*, 1736−1744.
(22) McCarthy, D. W.; Shefer, R. E.; Klinkowstein, R. E.; Bass, L. A.; Margeneau, W. H.; Cutler, C. S.; Anderson, C. J.; Welch, M. J. *Nucl. Med. Biol.* **1997**, *24*, 35−43.
(23) Perrier, S.; Takolpuckdee, P. *J. Polym. Sci., Part A: Polym. Chem.* **2005**, *43*, 5347−5393.
(24) Malkoch, M.; Thibault, R. J.; Drockenmuller, E.; Messerschmidt, M.; Voit, B.; Russell, T. P.; Hawker, C. J. *J. Am. Chem. Soc.* **2005**, *127*, 14942−14949.
(25) Fukukawa, K.-i. et. al. In preparation.
(26) Barner, L.; Davis, T. P.; Stenzel, M. H.; Barner-Kowollik, C. *Macromol. Rapid Commun.* **2007**, *28*, 539−559.
(27) Morrison, I. D.; Grabowski, E. F.; Herb, C. A. *Langmuir* **1985**, *1*, 496−501.
(28) Glinka, C. J.; Barker, J. G.; Hammouda, B.; Krueger, S.; Moyer, J. J.; Orts, W. J. *J. Appl. Crystallogr.* **1998**, *31*, 430−445.
(29) Kline, S. R. *J. Appl. Crystallogr.* **2006**, *39*, 895−900.
(30) Bartlett, P.; Ottewill, R. H. *J. Chem. Phys.* **1992**, *96*, 3306−3318.
(31) Rossin, R.; Pan, D.; Qi, K.; Turner, J. L.; Sun, X.; Wooley, K. L.; Welch, M. J. *J. Nucl. Med.* **2005**, *46*, 1210−1218.
(32) Sun, X.; Rossin, R.; Turner, J. L.; Becker, M. L.; Joralemon, M. J.; Welch, M. J.; Wooley, K. L. *Biomacromolecules* **2005**, *6*, 2541−2554.
(33) Yuan, J.; You, Y.; Lu, X.; Muzik, O.; Oupicky, D.; Peng, F. In preparation.
(34) Sun, X.; Anderson, C. J. *Methods Enzymol.* **2004**, *386*, 237−261.
(35) Hawker, C. J.; Bosman, A. W.; Harth, E. *Chem. Rev.* **2001**, *101*, 3661−3688.
(36) Matyjaszewski, K.; Xia, J. H. *Chem. Rev.* **2001**, *101*, 2921−2990.
(37) Alb, A. M.; Enohnyaket, P.; Drenski, M. F.; Shunmugam, R.; Tew, G. N.; Reed, W. F. *Macromolecules* **2006**, *39*, 8283−8292.
(38) Wang, Z.; He, J.; Tao, Y.; Yang, L.; Jiang, H.; Yang, Y. *Macromolecules* **2003**, *36*, 7446−7452.
(39) Jones-Wilson, T. M.; Deal, K. A.; Anderson, C. J.; McCarthy, D. W.; Kovacs, Z.; Motekaitis, R. J.; Sherry, A. D.; Martell, A. E.; Welch, M. J. *Nucl. Med. Biol.* **1998**, *25*, 523−530.
(40) Popielarski, S. R.; Hu-Lieskovan, S.; French, S. W.; Triche, T. J.; Davis, M. E. *Bioconjugate Chem.* **2005**, *16*, 1071−1080.
(41) Ota, Z.; Makin, H.; Takaya, Y.; Ofuji, T. *Renal Physiol.* **1980**, *3*, 317−323.
(42) Lee, C. C.; MacKay, J. A.; Frechet, J. M. J.; Szoka, F. C. *Nat. Biotechnol.* **2005**, *23*, 1517−1526.

BM700541E